

Fracture criterion for brick and mortar subjected to tri-axial state of stress

A. Litewka

Universidade da Beira Interior, Covilhã, Portugal

L. Szojda

Silesian University of Technology, Gliwice, Poland

ABSTRACT: The aim of the paper is to present experimental and theoretical study of fracture of brittle rock-like materials. To this end the tests of the specimens of brick and mortar subjected to various combinations of the tri-axial state of stress components were performed. The experiments made it possible to construct for both material tested the limit surfaces at material failure. The data obtained for brick and mortar subjected to uni-axial compression were used to calibrate the own theoretical model capable to describe the mechanical behavior of brittle materials. The limit surfaces obtained experimentally were compared with the theoretical predictions based on the fracture criterion proposed.

1 INTRODUCTION

Requirements of modern technology and progress in mechanics of solids and structures give rise to mutually interrelated extensive theoretical and experimental studies of mechanical properties of structural materials. Strong motivation for suitable oriented experiments exists in the case of brittle rock-like materials because of complexity of the phenomena that affect their mechanical response. Some results of experimental and theoretical studies of mechanical behavior of brittle rock-like materials have been previously reported mainly for uni-axial and bi-axial loading of concrete (Kupfer 1973, Ehm & Schneider 1985, Thienel et al. 1991, Ligeza 1999). Relatively small amount of respective experimental data for such materials subjected to tri-axial state of stress is available. Some data can be found in monographs on rock mechanics (Cristescu & Hunsche 1998, Derski et al. 1989, Goodman 1989) and on mechanics of concrete (Chen 1982, Neville 1995). Simultaneously new approach based on the methods of continuum damage mechanics has been used to formulate phenomenological models capable to describe the mechanical behavior of brittle rock-like materials in presence of oriented damage growth (Chaboche et al. 1995, Litewka et al. 1996, Murakami & Kamiya 1997, Halm and Dragon 1998). However, all those theoretical descriptions are based on limited experimental data, particularly for tri-axial state of stress and were verified for some specific cases of loading only. To obtain more realistic theoretical description of overall material response that could account for oriented damage

growth and development of damage induced anisotropy further extensive experimental studies are needed.

The aim of this paper is to supply experimental data on fracture of brick and mortar subjected to tri-axial state of stress as well as to show potentialities of own theoretical model (Litewka et al. 1996, Litewka & Dębiński 2003). A study of such a state of loading is a necessary first step towards analysis of complex conditions that are experienced by brick and mortar structures in practice during earthquakes or due to mining subsidence. That is why the tests were performed for relatively high values of the compressive mean normal stresses as well as for pure hydrostatic pressure.

2 EXPERIMENTS

The experiments presented here have been done as a continuation of those discussed by the authors in earlier paper (Litewka & Szojda 2006). The new results were obtained for specimens of the same types of mortar and brick that were tested earlier, and that is why the recent and older data could be compared. These two different series of the specimens are referred to as the specimens of Brick 1 and Mortar 1 for those reported in Litewka & Szojda (2006) and Brick 2 and Mortar 2 for these more recent presented here. The height and diameter of the cylindrical specimens used were equal to 12 cm and 6 cm, respectively. The specimens of brick were cut out from standard plain brick whereas those of mortar were prepared in special moulds. The details of the speci -

Table 1. Experimental data and constants used in theoretical analysis of tri-axial state of stress

Constant	Unit	Mortar	Brick
E_0	MPa	8730	2550
ν_0	-	0.173	0.103
f_c	MPa	-7.90	-10.85
A	MPa ⁻²	2095×10^{-5}	1249×10^{-5}
B	MPa ⁻²	62.55×10^{-5}	200.0×10^{-5}
C	MPa ⁻¹	-0.9469×10^{-5}	-1.100×10^{-5}
D	MPa ⁻¹	1.678×10^{-5}	3.754×10^{-5}
F	-	1.070	0.6900

mens preparation and the experimental procedure can be found elsewhere (Szojda 2001, Litewka & Szojda 2005).

The tests were performed for two cases of tri-axial compression referred to as State I and State II and also to pure hydrostatic pressure and uni-axial compression. The objective of the test performed under uni-axial compression was to calibrate the materials. That is why the initial Young modulus E_0 and Poisson ratio ν_0 as well as uni-axial compressive strength f_c were measured experimentally for both materials tested. The data shown in Table 1 were calculated as mean values measured for seven specimens of brick and seven for mortar. These values of standard constants E_0 , ν_0 , f_c and those for five other parameters A , B , C , D and F seen in Table 1 are necessary to employ the theoretical model proposed.

The objective of the tests under tri-axial state of stress was to measure the stresses at material fracture for prescribed loading programs. The tri-axial State I is a combination of uni-axial compression and hydrostatic pressure whereas the State II is a simultaneous action of hydrostatic pressure and uniform bi-axial compression. The respective stress ten-

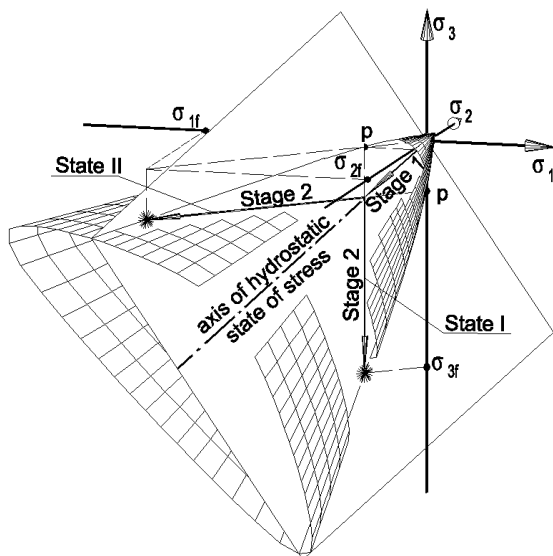


Figure 1. Limit surface at material fracture and loading paths for State I and State II: p point corresponding to material fracture.

Table 2. Experimental and theoretical failure stress for mortar subjected to State I of tri-axial compression.

Material	Specimen	Hydrostatic pressure, p MPa	Failure stress σ_{3f}	
			Experiment MPa	Theory MPa
Mortar 1	ZC1*	-1.04	-10.90	-13.32
	ZD1*	-0.934	-12.19	-12.83
	ZC2*	-1.84	-17.55	-16.71
	ZD2*	-1.92	-16.03	-17.01
	ZC3*	-2.69	-18.74	-19.77
	ZD3*	-2.92	-20.01	-20.56
Mortar 2	M-H4-1	-3.41	-25.59	-22.14
	M-H4-2	-4.33	-23.97	-24.89
	M-H8-2	-8.45	-39.85	-35.51
	M-H8-3	-8.20	-36.05	-34.92
	M-H12-1	-12.28	-48.34	-43.98
	M-H12-2	-12.37	-49.53	-44.17
M-H12-3	-11.95	-49.75	-43.29	

* The data for these specimens of Mortar 1 were discussed in Litewka & Szojda (2006).

Table 3. Experimental and theoretical failure stress for mortar subjected to State II of tri-axial compression.

Material	Specimen	Hydrostatic pressure, p MPa	Failure stress $\sigma_{1f} = \sigma_{2f}$	
			Experiment MPa	Theory MPa
Mortar 1	ZA1*	-0.01	-7.19	-8.60
	ZB1*	-0.21	-9.40	-10.98
	ZA2*	-2.30	-15.86	-21.74
	ZB2*	-2.37	-16.83	-22.01
	ZA3*	-3.81	-23.55	-26.79
	ZB3*	-3.92	-24.87	-27.12
Mortar 2	M-V0-1	-0.14	-11.47	-10.21
	M-V0-2	-0.09	-7.92	-9.64
	M-V2-1	-1.87	-21.69	-20.07
	M-V2-2	-2.29	-22.03	-21.71
	M-V4-1	-3.85	-24.50	-26.89
	M-V4-2	-4.46	-29.06	-28.70
	M-V8-1	-7.83	-29.43	-37.50
	M-V8-2	-8.00	-30.67	-37.90
	M-V12-1	-12.17	-44.22	-47.23
	M-V12-2	-11.63	-45.89	-46.07
	M-V12-3	-12.20	-44.75	-47.30

* The data for these specimens of Mortar 1 were discussed in Litewka & Szojda (2006).

Table 4. Experimental and theoretical failure stress for brick subjected to State II of tri-axial compression.

Material	Specimen	Hydrostatic pressure, p MPa	Failure stress $\sigma_{1f} = \sigma_{2f}$	
			Experiment MPa	Theory MPa
Brick 1	CA1*	0	-10.49	-10.96
	CB1*	-0.06	-14.36	-11.02
	CA2*	-2.76	-21.94	-22.87
	CB2*	-2.51	-17.19	-22.13
	CA3*	-3.34	-24.70	-24.46
	CB3*	-3.63	-22.83	-25.22
Brick 2	B-V9-1	-9.09	-36.21	-37.50
	B-V9-2	-9.26	-34.83	-37.85
	B-V9-3	-9.53	-31.56	-38.40

* The data for these specimens of Brick 1 were discussed in Litewka & Szojda (2006).

Table 5. Experimental and theoretical failure stress for brick subjected to State I of tri-axial compression.

Material	Specimen	Hydrostatic pressure, p MPa	Failure stress σ_{3f}	
			Experiment	Theory
			MPa	MPa
Brick 1	CC1*	-1.20	-15.27	-15.29
	CD1*	-0.93	-16.58	-14.29
	CC2*	-1.95	-20.86	-17.87
	CD2*	-2.13	-22.05	-18.45
	CC3*	-3.20	-22.23	-21.56
	CD3*	-3.03	-22.80	-21.09
Brick 2	B-H3-1	-3.14	-19.53	-21.40
	B-H3-2	-3.55	-21.56	-22.51
	B-H6-1	-6.64	-34.17	-29.87
	B-H6-2	-6.55	-33.66	-29.67
	B-H6-3	-6.30	-31.83	-29.12
	B-H9-1	-9.92	-47.26	-36.67
	B-H9-2	-8.66	-37.87	-34.13
	B-H9-3	-9.34	-40.68	-35.53

* The data for these specimens of Brick 1 were discussed in Litewka & Szojda (2006).

tor components that correspond to State I and State II are expressed by Equations (5), (6). Various combinations of the stress tensor components and at least two different loading paths are necessary to supply information on the shape of the limit surface at failure of the material subjected to tri-axial states of stress. The possible form of such a limit surface together with the loading paths for State I and State II of tri-axial compression is shown in Figure 1. It is seen from this figure that respective loading paths consisted of two stages. The Stage 1 was the same in both cases of tri-axial loading and consisted in a monotonic increase of hydrostatic pressure up to prescribed value p . In the Stage 2 of the first tri-axial state of stress (State I) the compressive vertical normal stress σ_V was increased up to material failure that occurs for $\sigma_{3f} = p + \sigma_V$. In the Stage 2 of the State II of tri-axial loading two compressive horizontal components σ_H of uniform bi-axial state of stress were increased simultaneously up to material failure that corresponds to $\sigma_{1f} = \sigma_{2f} = p + \sigma_H$. To obtain several combinations of the stress tensor components the various levels of the hydrostatic pressure p were used. The respective numerical data presented earlier (Litewka & Szojda 2006) as well as new ones are shown in Tables 2-5. The new experiments performed for Mortar 2 and Brick 2 according to the program seen in Tables 2-5 made it possible to determine the stresses at material fracture for higher levels of hydrostatic pressure p than those in earlier tests done for Mortar 1 and Brick 1.

3 FRACTURE CRITERION

The theoretical model of fracture and deformability of brittle rock-like materials employed in this paper, based on the assumption of tensorial nature of the

material damage was presented in earlier papers (Litewka et al. 1996, Litewka & Dębiński 2003, Litewka & Szojda 2006) and that is why the final form of the respective relations will be shown here. According to the rules of the continuum damage mechanics presented by Hayhurst (1983), Lemaitre (1984), Murakami (1987) and Krajcinovic (1995) the current state of the deteriorated material structure is described by the symmetric second rank damage tensor Ω_{ij} defined by Murakami & Ohno (1981) and Betten (1983). The explicit form of the relevant constitutive equations was found (Litewka et al. 1996, Litewka & Dębiński 2003) by employing the methods of the theory of tensor function representations as applied to solid mechanics by Boehler (1987) and Betten (1988, 1998). The first equation of the theoretical model is the stress-strain relation for anisotropic elastic solid

$$\varepsilon_{ij} = -\frac{\nu_0}{E_0} \delta_{ij} \sigma_{kk} + \frac{1+\nu}{E_0} \sigma_{ij} + C(\delta_{ij} D_{kl} \sigma_{kl} + D_{ij} \sigma_{kk}) + 2D(\sigma_{ik} D_{kj} + D_{ik} \sigma_{kj}), \quad (1)$$

where ε_{ij} is the strain tensor and σ_{ij} is the stress tensor. Equation (1) contains the Kronecker delta δ_{ij} , the Young modulus E_0 and Poisson ratio ν_0 for an originally undamaged material, two constants C and D to be determined experimentally and the second order modified damage tensor D_{ij} responsible for the current state of internal structure of the material defined by Litewka (1989).

Deterioration of the material structure due to applied load was described by the damage evolution equation expressed in the form of the tensor function

$$\Omega_{ij} = A s_{kl} s_{kl} (1 + H \det \boldsymbol{\sigma})^F \delta_{ij} + B \sqrt{\sigma_{kl} \sigma_{kl}} (1 + H \det \boldsymbol{\sigma})^F \sigma_{ij}, \quad (2)$$

where Ω_{ij} is a classical second order damage tensor formulated by Murakami & Ohno (1981) and Betten (1983), s_{kl} is the stress deviator, $\det \boldsymbol{\sigma}$ is the determinant of the matrix $\boldsymbol{\sigma}$ of the stress tensor σ_{ij} and A , B , F are material parameters to be determined experimentally. The multiplier H explained by Litewka & Dębiński (2003) and Litewka & Szojda (2006) is a function of the stress tensor components that was expressed by the following function of the stress tensor invariants

$$H = \frac{227}{200 |\det \boldsymbol{\sigma} + |(\sigma_{pp})^3|}. \quad (3)$$

Equation (3) is a result of detailed analysis of possible form of such a function of the stress tensor invariants necessary to fulfill the physical conditions discussed by Litewka & Szojda (2006).

The damage tensor Ω_{ij} that accounts for the continuity of the material is not sufficient to describe directly the overall macroscopic properties of dama-

ged material. That is why it was necessary to define a second order modified damage tensor D_{ij} capable to account for the strength and stiffness reduction of the damaged material. The relation

$$D_i = \frac{\Omega_i}{1 - \Omega_i}, \quad i = 1, 2, 3 \quad (4)$$

between the principal values Ω_1 , Ω_2 and Ω_3 of the damage tensor Ω_{ij} and the principal components D_1 , D_2 and D_3 of the modified damage tensor D_{ij} contained in Equation (1) was formulated by Litewka (1989). The principal components of the modified damage tensor (4) increase to infinity for fully damaged materials and that is why could reduce to zero the stiffness of the material expressed by Equation (1).

Theoretical model used in this paper can also be used to determine the maximum stresses that can be sustained by the material subjected to multi-axial state of stress. To this end the appropriate fracture criterion for brittle material was formulated according to the rules of the damage mechanics. The physical background of this criterion was looked for in the results of experiments done and in the failure modes of broken specimens. It is seen from Figure

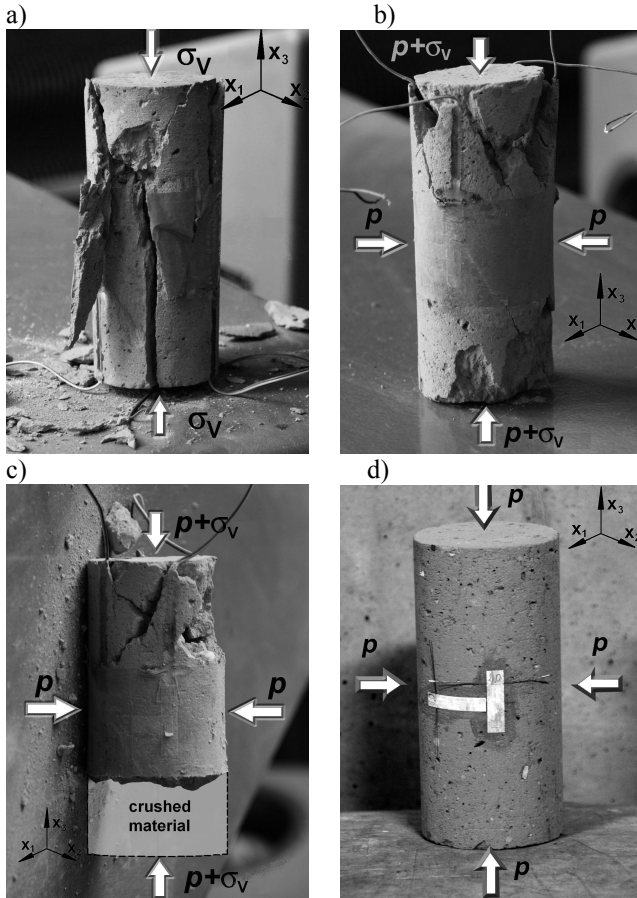


Figure 2. Specimens of bricks after tests: a) Specimen B-H0-2 tested under uni-axial compression, b) Specimen B-H3-2 tested under tri-axial compression, $p = -3.55$ MPa, c) Specimen B-H6-1 tested under tri-axial compression, $p = -6.64$ MPa, d) Specimen BC1 tested under pure hydrostatic compression.

2a that the failure of brick specimen subjected to uni-axial compression occurs due to accumulation and growth of vertical cracks. In the case of tri-axial compression shown in Figures 2b, c the material before its failure is totally crushed into separate tiny particles. This is well seen particularly in Figure 2c in the case of the specimen subjected to relatively high hydrostatic pressure p . In this specific case of loading the lower part of the specimen of brick is not seen in Figure 2c as it was completely crushed into powder whereas the other parts did not show so advanced degradation of the material structure. No photographs could be taken for three specimens of brick subjected to hydrostatic pressure $p = -9.92$, -8.66 and -9.34 MPa. These specimens were completely crushed into small particles and into powder. The similar failure modes were detected for the specimens of mortar where the total degradation of the internal structure occurred even for lower values of hydrostatic pressure. It means that tri-axial compression of brittle rock-like materials results in crack growth to such a state that at fracture the net cross section area on certain planes is reduced to zero. This full deterioration of internal structure of the material occurs when at least one of the principal components Ω_1 , Ω_2 or Ω_3 of the damage tensor Ω_{ij} determined from Equation (2) reaches the limit value equal to unity.

To compare the experimental results with theoretical prediction the Equation (2) was expressed in terms of the stress tensors components

$$\sigma_{ij} = \begin{bmatrix} \sigma_{11} = p & 0 & 0 \\ 0 & \sigma_{22} = p & 0 \\ 0 & 0 & \sigma_{33} = \sigma_V + p \end{bmatrix} \quad (5)$$

for State I of tri-axial compression and

$$\sigma_{ij} = \begin{bmatrix} \sigma_{11} = \sigma_H + p & 0 & 0 \\ 0 & \sigma_{22} = \sigma_H + p & 0 \\ 0 & 0 & \sigma_{33} = p \end{bmatrix} \quad (6)$$

for State II of tri-axial compression. Taking into account the notation adopted in Equation (5) the relation

$$\Omega_1 = \Omega_2 = \left(\frac{2}{3} A \sigma_V^2 + B p \sqrt{\sigma_V^2 + 2 \sigma_V p + 3 p^2} \right) \cdot \left[1 + \frac{227(\sigma_V + p)p^2}{200|(\sigma_V + p)p^2| + |(\sigma_V + 3p)^3|} \right]^F = 1. \quad (7)$$

was obtained for State I. The third principal component of the damage tensor Ω_3 does not decide in this case on the material fracture as it grows slower than Ω_1 and Ω_2 . The State II of tri-axial compression expressed by Equation (6) is characterized by faster

growth of the principal component Ω_3 of the damage tensor and that is why the material fracture occurs when

$$\Omega_3 = \left(\frac{2}{3} A \sigma_H^2 + B p \sqrt{2\sigma_H^2 + 4\sigma_H p + 3p^2} \right) \cdot \left[1 + \frac{227(\sigma_H + p)^2 p}{200 |(\sigma_H + p)^2 p| + |(2\sigma_H + 3p)^3|} \right]^F = 1. \quad (8)$$

In this case the growth of two others principal components Ω_1 and Ω_2 of the damage tensor is slower and that is why they do not decide about the onset of fracture.

Application of the fracture criterion proposed requires calibration of the material. The numerical values of the constants A , B , C , D and F shown in Table 1 were obtained by using the stress-strain curves determined experimentally for uni-axial compression of brick and mortar seen in Figures 3, 4.

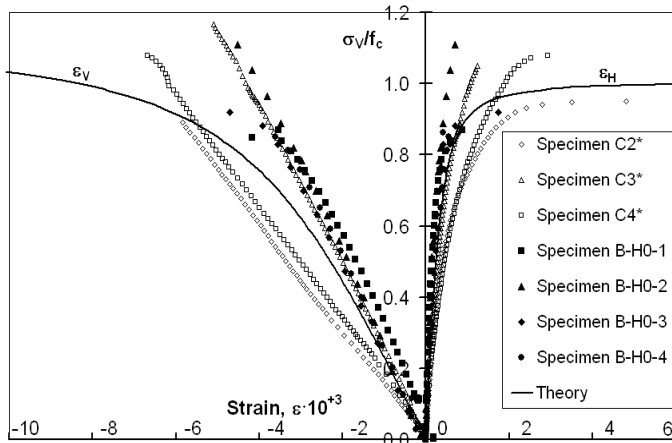


Figure 3. Experimental and theoretical stress-strain curves for brick subjected to uni-axial compression.

* The data for these specimens of Brick 1 were used in Litewka & Szojda (2006).

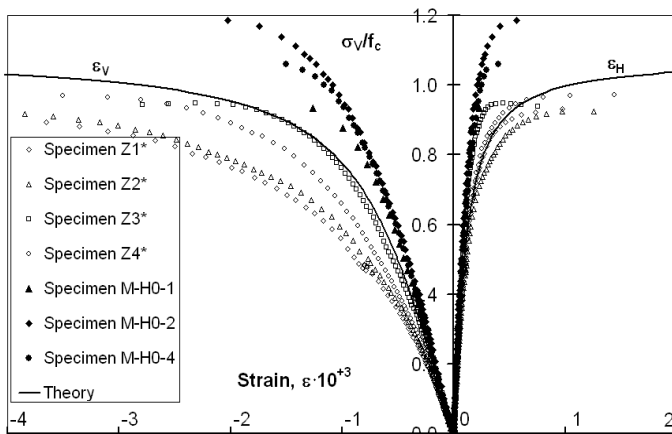


Figure 4. Experimental and theoretical stress-strain curves for mortar subjected to uni-axial compression.

* The data for these specimens of Mortar 1 were used in Litewka & Szojda (2006).

The details of the method used here to identify the material parameters have been described by Litewka & Dębiński (2003). The constant F that appears in Equations (2), (7), (8) was also determined experimentally and to do this, one point taken from one stress-strain curve obtained experimentally for tri-axial compression is sufficient. Theoretical stress-strain curves shown in Figures 3, 4 were obtained from the relations

$$\varepsilon_1 = \varepsilon_2 = \varepsilon_H = -\frac{\nu_0}{E_0} \sigma_V + C \left[\frac{2A\sigma_V^3 - 3B\sigma_V^3}{3 - 2A\sigma_V^2 + 3B\sigma_V^2} + \frac{2A\sigma_V^3}{3 - 2A\sigma_V^2} \right] \quad (9)$$

$$\varepsilon_3 = \varepsilon_V = \frac{\sigma_V}{E_0} + (2C + 4D) \frac{2A\sigma_V^3 - 3B\sigma_V^3}{3 - 2A\sigma_V^2 + 3B\sigma_V^2}. \quad (10)$$

Equations (9), (10) were obtained by specifying the stress-strain relation (1) for uni-axial compression.

Equations (7) and (8) were used to calculate the values of σ_V and σ_H corresponding to material failure in State I and State II. These data made it possible to determine the theoretical stresses at material fracture $\sigma_{3f} = p + \sigma_V$ for State I and $\sigma_{1f} = \sigma_{2f} = p + \sigma_H$ for State II. Comparison of these theoretical predictions with corresponding experimental data for mortar and brick is shown in Tables 2-5.

4 DISCUSSION OF THE RESULTS

Experimental results obtained for tri-axial loading of the specimens of mortar and brick made it possible to determine the configuration of the stress tensor components at material failure. The experimental data for State I and State II shown in Tables 2-5 were used to determine the limit surfaces at material fracture. The form of such limit surface for brittle rock-like materials, constructed at the stress space (Willam and Warnke, 1975; Szojda, 2001) is shown in Figures 1, 5, 6. The axes of the coordinate system shown in Figure 1 correspond to the principal stresses σ_1 , σ_2 , σ_3 whereas those in Figures 5, 6 are defined by the mean stress

$$\sigma_m = \frac{\sigma_{11} + \sigma_{22} + \sigma_{33}}{3} \quad (11)$$

and stress intensity

$$\sigma_i = \left\{ \frac{1}{2} \left[(\sigma_{11} - \sigma_m)^2 + (\sigma_{22} - \sigma_m)^2 + (\sigma_{33} - \sigma_m)^2 \right] + \tau_{12}^2 + \tau_{23}^2 + \tau_{31}^2 \right\}^{0.5}, \quad (12)$$

where σ_{11} , σ_{22} , σ_{33} , τ_{12} , τ_{23} and τ_{31} are the stress tensor components. The meridians of the limit surface seen in Figures 5, 6 can be divided into three

parts. Tri-axial tests presented in this paper made it possible to study experimentally the main almost rectilinear part of the meridian that corresponds to negative mean stresses. To this end the experimental results presented in Tables 2-5 for both materials subjected to State I and State II of tri-axial loading and also those obtained for the specimens of each material subjected to uni-axial compression were used. The experimental study of region of positive mean stresses where failure occurs in brittle manner by fracture of the material requires multi-axial tensile tests which are very difficult in the case of brittle rock-like materials. To obtain any experimental data for third region of large negative mean stresses where failure occurs by particle crushing, the tri-axial tests should be performed at very high values of hydrostatic pressure p combined with uni-

Table 6. Specimens of mortar and brick tested under pure hydrostatic pressure.

Mortar 2		Brick 2	
Specimen	Hydrostatic pressure, p MPa	Specimen	Hydrostatic pressure, p MPa
MC1	-64.8	BC1	-65.9
MC2	-66.3	BC2	-66.9
MC3	-64.3	BC3	-65.1

axial compression (State I) or uniform bi-axial compression (State II).

Theoretical model (Litewka & Dębiński 2003, Litewka & Szojda 2006) applied in this paper can also be used to determine the form of the limit surface at material failure. The respective theoretical

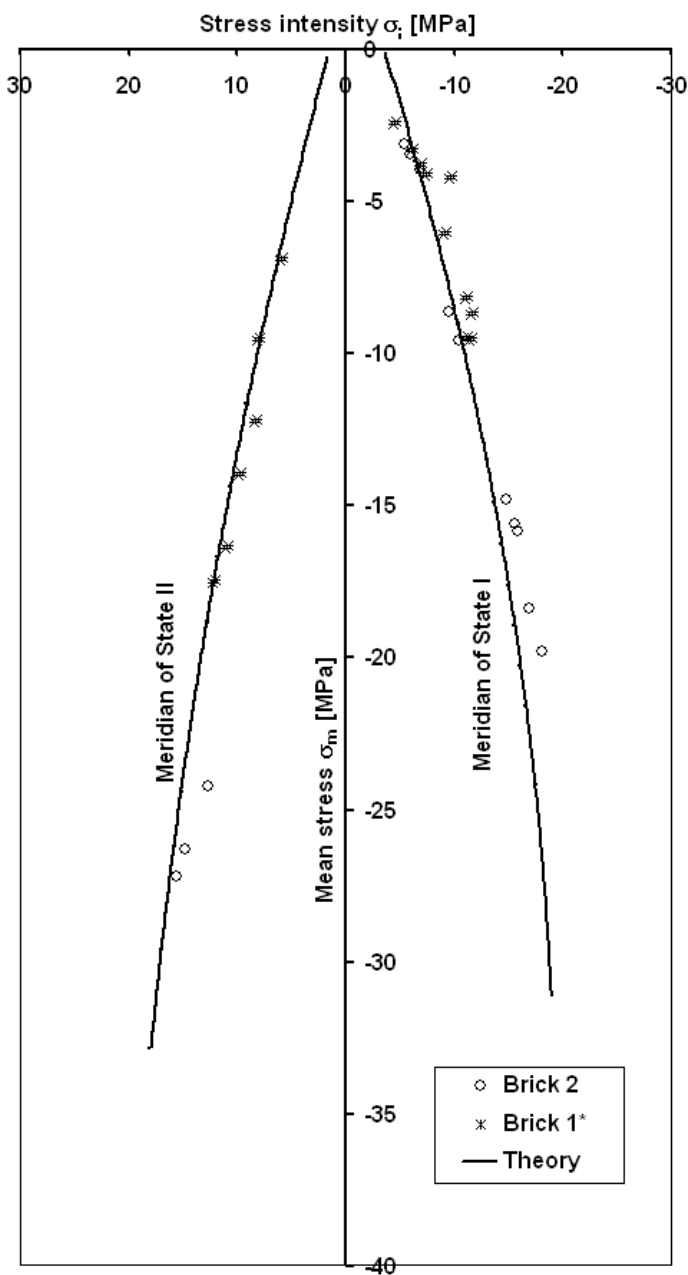


Figure 5. Main meridians of limit surface at fracture for brick. * These data for Brick 1 were discussed in Litewka & Szojda (2006).

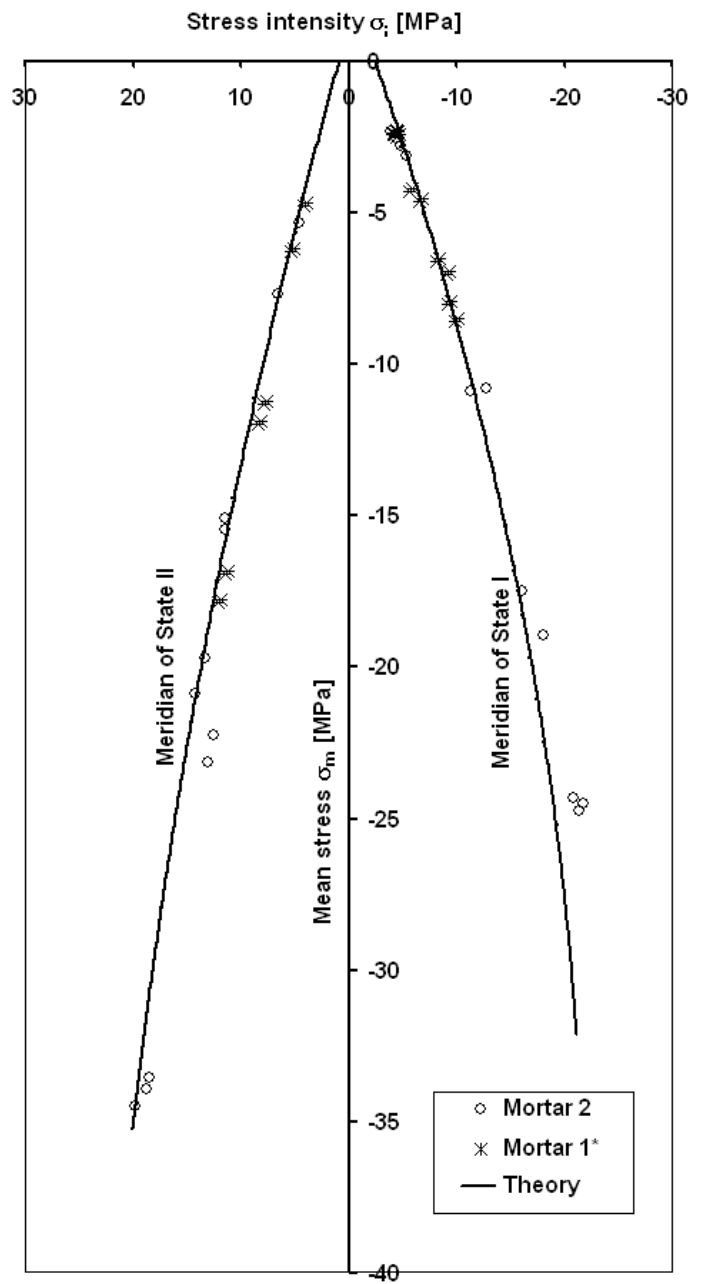


Figure 6. Main meridians of limit surface at fracture for mortar. * These data for Mortar 1 were discussed in Litewka & Szojda (2006).

results obtained from Equations (7), (8), (11), (12) were used to construct the meridians of the theoretical limit surfaces for brick and mortar. Fairly good agreement of the theoretical predictions with experimental data is seen in Figures 5, 6. The meridians of the limit surfaces for both materials become curvilinear for negative mean stresses larger than $3f_c$. It could suggest that the specimens subjected to very high values of pure hydrostatic pressure could fail and the limit surface might be closed for certain sufficiently large mean stresses.

To obtain any experimental evidence that the limit surface would really be closed for negative mean stresses it should be necessary to do the tests at extremely high hydrostatic pressure. The experimental study of this problem was also attempted here. To this end three specimens of the Brick 2 and three specimens of Mortar 2 were tested under pure hydrostatic pressure up to the limit capacity of the testing machine. For the machine used in these experiments the maximum hydrostatic pressure was equal to $p = -70$ MPa. The list of the specimens tested and respective maximum values of p applied is shown in Table 6. All the specimens during the process of loading did not show any symptoms of failure. Moreover, inspection of the specimens after unloading did not reveal any degradation of the internal structure. This can be seen in Figure 2d where the photograph of the specimen BC1 after loading up to $p = -65.9$ MPa and unloading is presented. The results of these experiments and also of those similar reported for concrete by Neville (1995) suggest that this region of limit surface is out of the range of actually existing testing machines.

5 CONCLUSIONS

Experiments on behavior of brick and mortar under tri-axial loading presented in the paper were used to study the fracture of brittle materials subjected to higher values of negative mean stresses than those applied in earlier tests. The shape of theoretical limit surface at material failure was determined and compared with the experimental data obtained. Fairly good agreement of the experimental data and theoretical predictions was detected for both materials tested. Increasing compressive strength of brittle rock-like materials known from earlier experiments for specimens of rocks and soils subjected to confined axial compression was also observed in second tri-axial test used here. The experiments performed under pure hydrostatic pressure up to $p = 8f_c$ did not show any evidence that the limit surface for such a level of negative mean stresses might be closed. All these phenomena can also be explained theoretically within the mathematical model proposed. Thus, the experimental technique adopted and phenomenolo-

gical model used in this paper proved to be accurate enough to study the shape of the limit surface at material failure.

ACKNOWLEDGEMENTS

This work was done within the F.C.T. Program C.E.C. U.B.I. and was financially supported by KBN Grant 5 T07E 028 25 and EC contract MTKD-CT-2004-509775.

REFERENCES

- Betten, J. 1983. Damage tensors in continuum mechanics. *Journal of Méchanique Théorique et Appliquée* 2(1): 13-32.
- Betten, J. 1988. Applications of tensor functions to the formulation of yield criteria for anisotropic materials. *International Journal of Plasticity* 4(1): 29-46.
- Betten, J. 1998. Anwendungen von Tensorfunktionen in der Kontinuumsmechanik anisotroper Materialien. *Zeitschrift für Angewandte Mathematik und Mechanik* 78(8): 507-521.
- Boehler, J.P. 1987. *Applications of tensor functions in solid mechanics*. Wien: Springer-Verlag.
- Chaboche, J.L., Lesne, P.M. & Maire, J.F. 1995. Continuum damage mechanics, anisotropy and damage deactivation for brittle materials like concrete and ceramic composites. *International Journal of Damage Mechanics* 4(1): 5-22.
- Chen, W.F. 1982. *Plasticity of reinforced concrete*. New York: McGraw-Hill.
- Cristescu, N.D. & Hunsche, U. 1998. *Time effects in rock mechanics*. Chichester: John Wiley & Sons.
- Derski, W., Izbicki, R., Kisiel, I. & Mroz, Z. 1989. *Rock and soil mechanics*. Amsterdam-Warsaw: Elsevier-P.W.N.
- Ehm, C. & Schneider, U. 1985. Biaxial testing of reactor concrete. In *Transactions of 8th International Conference on Structural Mechanics in Reactor Technology*: Vol. H 349-354. Bruxelles: North Holland.
- Goodman, R.E. 1989. *Introduction to rock mechanics*. New York: John Wiley & Sons.
- Halm, D. & Dragon A. 1998. An anisotropic model of damage and frictional sliding for brittle materials. *European Journal of Mechanics A/Solids* 17(3): 439-460.
- Hayhurst, D.R. 1983. On the role of creep continuum damage in structural mechanics. In B. Wilshire & D.R.J. Owen (eds.), *Engineering Approaches to High Temperature Design*: 85-175. Swansea: Pineridge Press.
- Krajcinovic, D. 1995. Continuum damage mechanics: when and how?. *International Journal of Damage Mechanics* 4(3): 217-229.
- Kupfer, H. 1973. Das Verhalten des Betons unter mehrachsiger Kurzzeitbelastung unter besonderer Berücksichtigung der zweiachsigen Beanspruchung. In *Deutscher Ausschuss für Stahlbeton*, 229: 1-105. Berlin: Wilhelm Ernst & Sohn.
- Lemaitre, J. 1984. How to use damage mechanic. *Nuclear Engineering and Design* 80: 233-245.
- Ligeza, W. 1999. Experimental stress-strain relationship for cement concrete under biaxial compression. In *Proceedings of the International Conference, Concrete and Concrete Structures*: 47-54, Zilina.
- Litewka, A. 1989. Creep rupture of metals under multi-axial state of stress. *Archives of Mechanics* 41(1): 3-23.
- Litewka, A., Bogucka, J. & Dębiński, J. 1996. Deformation induced anisotropy of concrete. *Archives of Civil Engineering* 42(4): 425-445.

- Litewka, A. & Dębiński, J. 2003. Load-induced oriented damage and anisotropy of rock-like materials. *International Journal of Plasticity* 19(12): 2171-2191.
- Litewka, A. & Szojda L. 2005. Triaxial tests for brittle materials: motivation, technique, results. *Civil and Environmental Engineering Reports* 1: 169-188.
- Litewka, A. & Szojda, L. 2006. Damage, plasticity and failure of ceramics and cementitious composites subjected to multi-axial state of stress. *International Journal of Plasticity* 22(11): 2048-2065.
- Murakami, S. 1987. Progress in continuum damage mechanics. *JSME International Journal* 30: 701-710.
- Murakami, S. & Kamiya, K. 1997. Constitutive and damage evolution equations of elastic-brittle materials based on irreversible thermodynamics. *International Journal of Mechanical Sciences* 39(4): 473-486.
- Murakami, S. & Ohno, N., 1981. A continuum theory of creep and creep damage. In A.R.S. Ponter & D.R. Hayhurst, (eds.), *Creep in Structures*: 422-444. Berlin: Springer-Verlag.
- Neville, A.M. 1995. *Properties of concrete*. Harlow: Longman.
- Szojda L. 2001. *Analysis of interaction of masonry structures and deformable foundation*, PhD Thesis, Silesian University of Technology, Gliwice, (in Polish).
- Thienel, K.-Ch., Rostasy, F.S. & Becker, G. 1991. Strength and deformation of sealed HTR-concrete under biaxial stress at elevated temperature. In *Transactions of 11th International Conference Structural Mechanics in Reactor Technology*: Vol. H 73-78. Tokyo: Atomic Energy Society of Japan.
- Willam, K. J. & Warnke, E. P. 1975. Constitutive Models for the Triaxial Behavior of Concrete, *Proc. of IABSE Report 19*: 1-30, Zürich.